Solid State Sciences 14 (2012) 1050–1054

Contents lists available at SciVerse ScienceDirect

Solid State Sciences

journal homepage: www.elsevier.com/locate/ssscie

Fabrication of PtRu/Ru core–shell nanowires by exchanging Ru phases

Geon-Hyoung An, Hyo-Jin Ahn*

Department of Materials Science and Engineering, Seoul National University of Science and Technology, 172 Gongreung 2-dong, Nowon-gu, Seoul 139-743, Republic of Korea

ARTICLE INFO

Article history:
Received 21 September 2011
Received in revised form
2 February 2012
Accepted 20 May 2012
Available online 27 May 2012

Keywords:
Core–shell nanowires
Co-electrospinning
Pt
Ru
Formation mechanism
Interdiffusion

ABSTRACT

In this study, we successfully fabricated PtRu/Ru core–shell nanowires (NWs) prepared from as-spun Ru/Pt core–shell NWs via a co-electrospinning method. Their formation mechanism together with the structural characteristics, morphology, and composition of the resulting PtRu/Ru core–shell NWs was elucidated by means of scanning electron microscopy (SEM), transmission electron microscopy (TEM) with energy dispersive X-ray spectroscopy (EDS), and X-ray diffraction (XRD). PtRu/Ru core–shell NWs fabricated from as-spun Ru/Pt core–shell NWs were formed as a result of interdiffusion between Ru atoms and Pt atoms during calcination after co-electrospinning.

1. Introduction

Nanostructured materials are of considerable interest because of their unique physical, electronic, and chemical properties as compared to their bulk counterparts [1]. In particular, one-dimensional nanostructured materials such as nanowires, nanotubes, nanobelts, and nanorods have recently gained burgeoning attention owing to such applications as energy storage devices, biological sensors, catalysis, optoelectronics, and electronics, as well as to their unique applications with nanoscale devices when compared to zero-dimensional nanostructured materials [2,3]. Currently, various synthetic methods, including template-direct synthesis, solvothermal methods, hydrothermal methods, chemical vapour deposition, and electrospinning, are used to fabricate one-dimensional nanostructured materials. Among the various methods, electrospinning has recently become a popular technique for generating various NWs, including polymer, composite, ceramic, and carbon NWs; this method also offer many advantages, such as its simple process, large-scale production, and controllability of morphology in the NWs [4–6]. A typical electrospinning apparatus, as shown in Scheme 1, is composed of a high voltage power supply, a syringe with pump, and a collector (counter electrode). More recently, co-electrospinning, which is set up with two coaxial capillaries, as shown in the enlarged schematic of Scheme 1, has been developed for fabricating core–shell NWs or hollow NWs [7–10]. For example, Li et al. reported on the synthesis of TiO_2 hollow NWs using a coaxial, two-capillary spinneret in electrospinning together with control of various experimental parameters [8]. Chen et al. reported that nanowire-in-microtube structured core–shell fibres with homogenous or heterogeneous fibres were fabricated via multifluidic coaxial electrospinning for such applications as optics and microelectronics [9]. Sun et al. synthesised and described compound core–shell polymer NWs, such as PEO(shell)–PDT(core) and PEO(shell)–PSU(core), fabricated by co-electrospinning of two materials [10]. In addition, Kim et al. reported that binary metallic NWs of PtRh and PtRu alloy via a single-electrospinning method were fabricated and demonstrated their methanol electrooxidation for use in direct methanol fuel cells (DMFCs) [11]. In this context, morphology modification of one-dimensional nanostructures such as core–shell NWs, hollow NWs, and binary metallic NWs, can further improve material properties relative to chemistry, physics, and electrochemistry for the above-mentioned applications. Therefore, understanding of the formation mechanism and the morphology modification for one-dimensional nanostructures is very important, but this understanding is currently inadequate. Furthermore, the exchange of two different phases in core–shell NWs has hitherto not been reported.

In this study, we successfully fabricated PtRu/Ru core–shell NWs via a co-electrospinning technique and elucidated their

* Corresponding author. Tel.: +82 02 9706622; fax: +82 02 9736657.
E-mail address: hjahn@seoultech.ac.kr (H.-J. Ahn).

1293-2558/$ – see front matter © 2012 Elsevier Masson SAS. All rights reserved.
doi:10.1016/j.solidstatesciences.2012.05.017

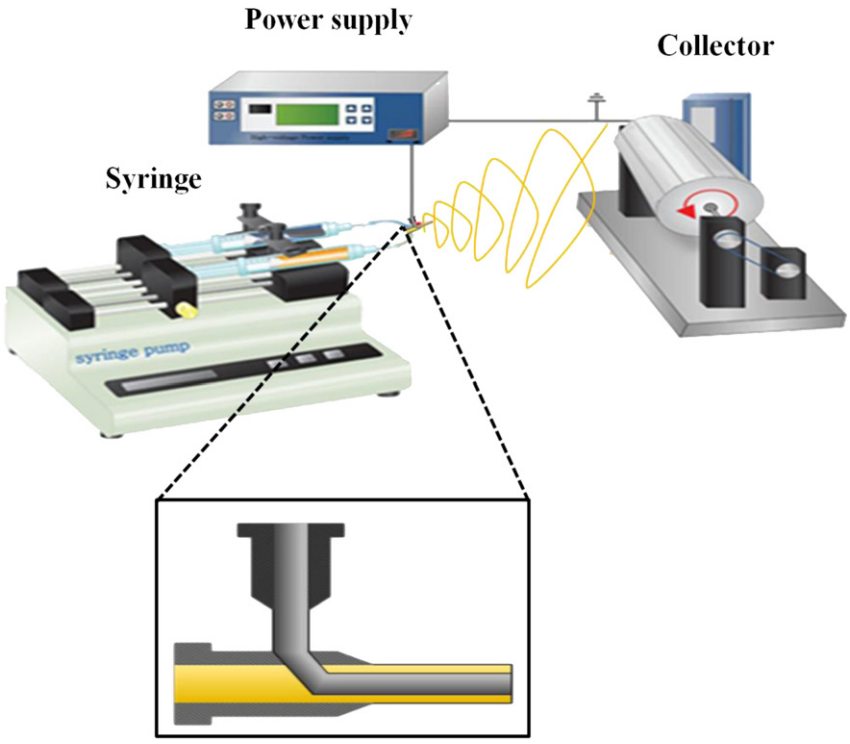

Scheme 1. Co-electrospinning apparatus consisting of a high voltage power supply, a syringe with pump, and a collector (counter electrode). Enlarged schematic exhibits two coaxial capillaries for fabricating the core–shell NWs.

formation mechanism by means of SEM, TEM, EDS, and XRD. In addition, the PtRu/Ru core–shell NWs can be used as applications such as catalysts, fuel cells, and electrochemical sensors [12–14].

2. Experimental method

To make PtRu/Ru core–shell NWs, as-spun Ru/Pt core–shell NWs composited with PVP polymer were first fabricated via co-electrospinning. After setting up two coaxial capillaries, two precursor solutions for use in the core region and the shell region were prepared one by one. First, in the case of the core region, 10 wt % of ruthenium chloride hydrate ($RuCl_3 \cdot xH_2O$, Aldrich) was dissolved in *N*,*N*-Dimethylformamide (Aldrich), and then poly(-vinylpyrrolidone) (PVP, Mw = 1,300,000 g/mol, Aldrich) was added. In the case of the shell region, 1, 4, 7, and 13 wt% of chloroplatinic acid hydrate ($H_2PtCl_6 \cdot xH_2O$) (referred to as samples A, B, C, and D) were dissolved in DI water for 5 h. Then, the poly(vinylpyrrolidone) (PVP, Mw = 1,300,000 g/mol, Aldrich) solution dissolved in ethanol (Alfa Aesar) was mixed with the above-dispersed solution for 1 h. The two coaxial capillaries consisted of a 26 gauge inner capillary and an 18 gauge outer capillary. The distance between syringe needle and collector was fixed at ~17 cm, and the feeding rate of the inner solution and of the outer solution were 0.01 ml/h and 0.02 ml/h, respectively. An applied voltage was maintained at ~15 kV for sample A, and ~20 kV for sample B, C, and D. Then, the resulting as-spun NWs were dried at 70 °C for 2 h and calcined at 400 °C for 2 h. The resulting core–shell NWs were heat-treated using a gas mixture (N_2:H_2 = 90%:10%) at 150 °C for 0.5 h to transform from RuO_2 phases to Ru phases.

The structure and morphology of the NWs was analysed using scanning electron microscopy (SEM, Hitach S-4700) and transmission electron microscopy (TEM, TECNAI F-20) with SAED (selected area electron diffraction) patterns. TEM-EDS mapping data were obtained using a Phillips CM20T/STEM electron microscope equipped with energy dispersive X-ray spectroscopy (EDS). The structural properties of the NWs were measured using an X-ray diffraction (XRD, Rigaku D/Max 2500 V equipped with a Cu K_α source) technique.

3. Results and discussion

Fig. 1(a)–(e) shows FESEM images of single RuO_2 NWs, sample A, sample B, sample C, and sample D, respectively. To investigate the formation mechanism of the PtRu/Ru core–shell NWs, we studied four different types of samples, which were controlled as four different weight percentages (1, 3, 7, and 13 wt%) of Pt and a constant weight percentage (10 wt%) of Ru. Fig. 1(a) presents SEM images obtained from the single RuO_2 NWs after calcination at 400 °C for 2 h. The single RuO_2 NWs, which were fabricated using one capillary, are in the range of ~67 nm–~76 nm in diameter and rough surfaces are apparent on the NWs. As shown in Fig. 1, the diameters of sample A, sample B, sample C, and sample D gradually increased with increasing amounts of Pt; the diameters are in the ranges of ~70 nm–~105 nm, ~83 nm–~126 nm, ~113 nm–~150 nm, and ~167 nm–~350 nm, respectively. In addition, as shown in the insets of Fig. 1, the surface roughness properties of the NWs gradually become smooth in accordance with the increased diameter of the NWs.

Fig. 2(a)–(d) presents bright-field TEM images and SAED patterns for sample A, sample B, sample C, and sample D before calcination. The diameters of the NWs gradually increase with increased amounts of Pt; ~120 nm for sample A, ~137 nm for sample B, ~160 nm for sample C, and ~210 nm for sample D. All the samples before calcination exhibit uniform contrast in the entire area of the NWs. In particular, SAED data for all the NWs exhibit a broad diffuse ring around the (000) spot, which indicates an amorphous characteristic of the NWs. The as-spun core–shell

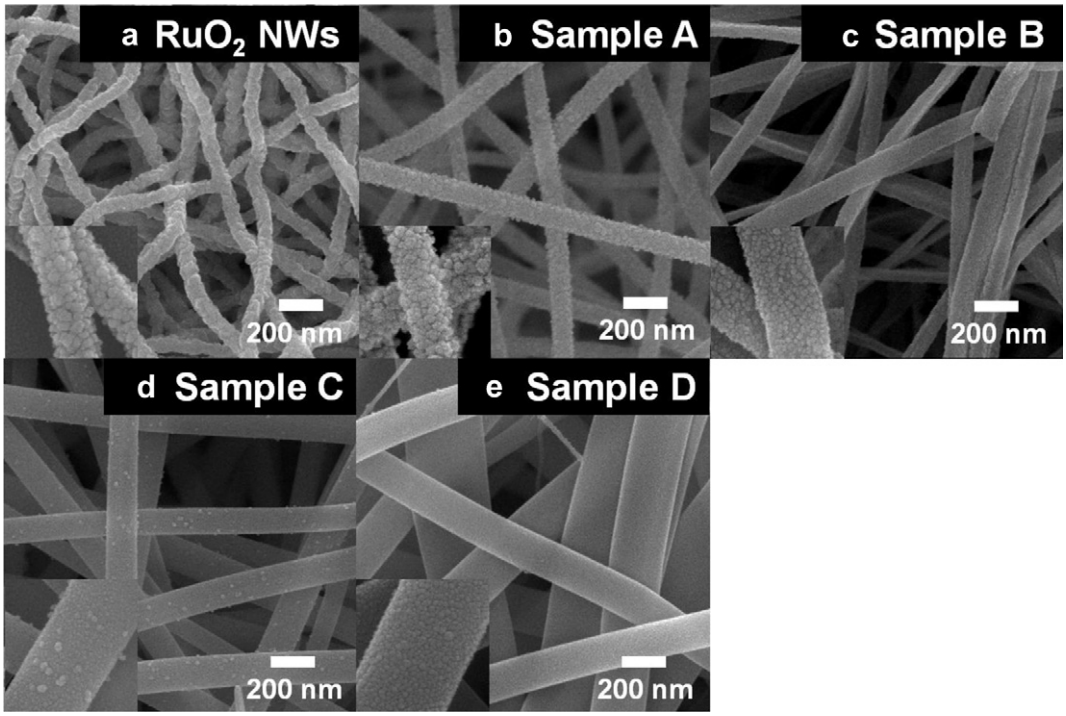

Fig. 1. SEM images of single RuO_2 NWs, sample A, sample B, sample C, and sample D after calcination.

NWs before calcination consist of Ru metal precursor-PVP composite NWs in the core region and Pt metal precursor-PVP composite NWs in the shell region fabricated by co-electrospinning. For the core region in two coaxial capillaries before calcination, as-spun ruthenium metal precursor-PVP composite NWs are synthesised as the type of Ru^{3+}–PVP formed by the interaction between the carbonyl oxygen of PVP and the Ru^{4+} of ruthenium chloride hydrate. For the shell region, as-spun platinum metal precursor-PVP composite NWs are synthesised as the type of Pt^{4+}–PVP formed by the interaction between the carbonyl oxygen of PVP and the Pt^{4+} of chloroplatinic acid hydrate. Here, PVP is added as a stabiliser to ensure the fabrication of uniform NWs. Furthermore, the TEM image of sample D in Fig. 2(d) reveals bright band-like contrast in the edge area of the NWs relative to the Pt metal precursor-PVP composite NWs. This will be discussed in detail in relation to the TEM-EDS

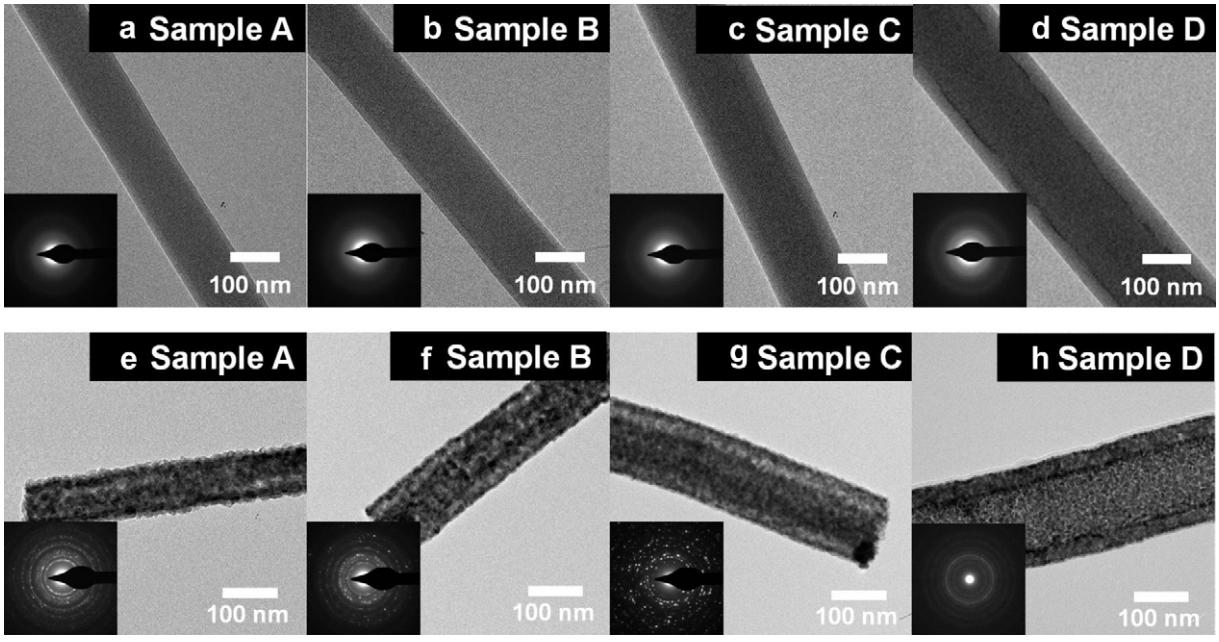

Fig. 2. TEM images and SAED patterns for sample A, sample B, sample C, and sample D before calcination (a)–(d) and after calcination (e)–(h).

mapping data of Fig. 3. Fig. 2(e)–(h) presents TEM images and SAED patterns obtained from sample A, sample B, sample C, and sample D, respectively, after calcination at 400 °C for 2 h. SAED patterns, as shown in the insets of Fig. 2(e)–(h), exhibit sharp diffuse ring patterns around the (000) spot, implying a poly-crystalline characteristic of the NWs. The diameters of all the NWs were reduced to ~20% of the diameters of the as-spun NWs, as shown in Fig. 2, owing to the removal of PVP polymer during calcination after co-electrospinning. Thus, the diameters of sample A, sample B, sample C, and sample D are ~100 nm, ~120 nm, ~140 nm, and ~190 nm, respectively. All the NWs exhibit rough morphology on their surface owing to the removal of PVP polymer. In particular, a band-like region of ~40 nm in size for sample D was clearly formed, and core–shell NWs were successfully fabricated.

To confirm the composition of the core–shell NWs, TEM-EDS mapping examinations were performed for sample A before and after calcination, as shown in Fig. 3. The EDS results indicate that Pt and Ru atoms are uniformly distributed in the NWs. In the case of the NWs before calcination (see Fig. 3(a)), the distribution of Pt atoms is slightly larger than that of Ru atoms. This implies that the core and shell regions of the NWs consist of Ru phases and Pt phases. However, in the case of the NWs after calcination (see Fig. 3(b)), the distribution of Pt atoms is smaller than that of Ru atoms, implying that the core and shell regions of the NWs consist of Pt phases and Ru phases. This could be explained by the inter-diffusion phenomenon, i.e., Pt atoms in the shell region of the NWs before calcination move into core region and Ru atoms in the core region of the NWs move into the shell region during calcination at 400 °C in air. Ru atoms tend to oxidise preferentially compared to Pt atoms. Thus, Ru atoms should be moved by diffusion from the core region to the shell region to encounter oxygen during calcination in air, owing to lower Gibbs free energy of formation. On the other hand, Pt atoms co-occur to interdiffuse into the core region owing to the easy formation of PtRu alloys [15]. As previously reported [16], the Pt phases can be alloyed until almost 60 atom % of Ru in the alloy with faced-centred cubic structure. As a result, Pt atoms move into the core region and Ru atoms move into the shell region of the NWs. That is, in the case of all the NWs, the core region and the band-like region were formed to Pt phases and Ru phases after

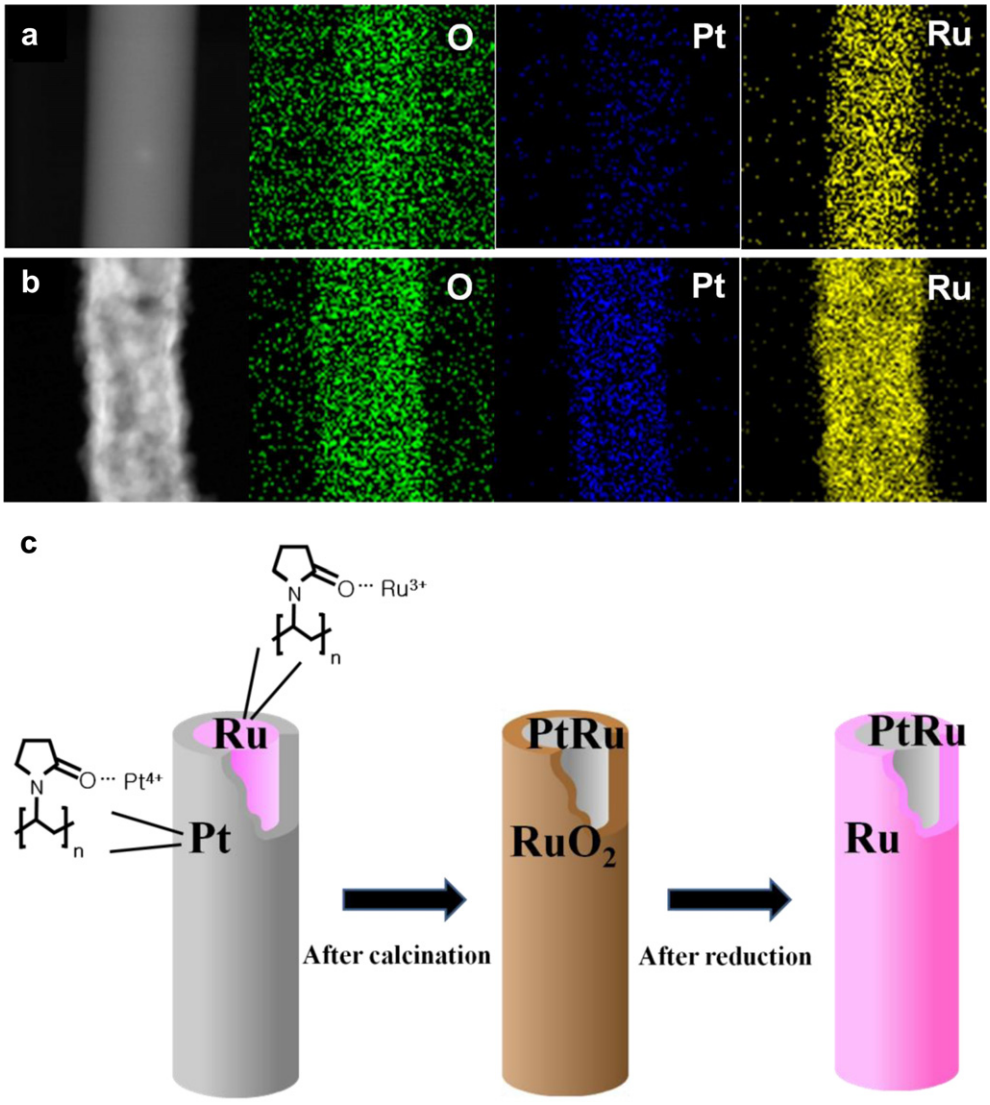

Fig. 3. TEM-EDS mapping data of sample A before calcination (a) and after calcination (b); a schematic illustration to produce the PtRu–Ru core–shell NWs fabricated from as-spun Ru–Pt core–shell NWs (c).

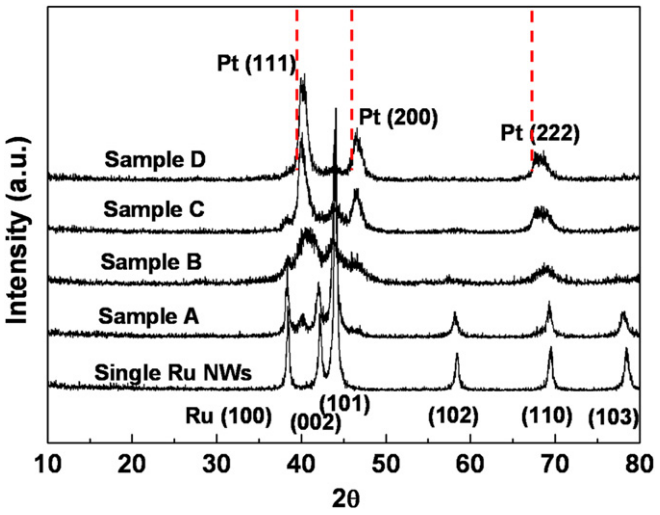

Fig. 4. Powder XRD plots obtained from single Ru NWs, sample A, sample B, sample C, and sample D after the reduction process.

calcination. Furthermore, after calcination at 400 °C for 2 h in air, a reduction process at 150 °C for 0.5 h was performed under H_2 gas (N_2:H_2 = 90%:10%) to obtain metallic PtRu/Ru core–shell NWs. Finally, metallic PtRu/Ru core–shell NWs were successfully fabricated using a co-electrospinning technique together with reduction process, which is explained by a schematic illustration, to produce the core–shell NWs, as shown in Fig. 3(c).

To further investigate the structural properties of the NWs, XRD examinations were carried out as shown in Fig. 4. Fig. 4 presents powder XRD plots obtained from single RuO_2 NWs, sample A, sample B, sample C, and sample D after the reduction process. For the Ru NWs, 38.3°, 42.1°, 44.0°, 58.3°, 69.4°, and 78.3° correspond to the (110), (002), (101), (102), (110), and (103) plane, indicating metallic Ru phase with hexagonal structure (space group $p6_3/mmc$ [194]) (JPCDS No. 06-0663). The diffraction peaks of the Pt phases increased as the amount of Pt increased, while the diffraction peaks of the Ru phases decreased. In addition, the (111), (200), and (220) plane of the Pt phases, which have face-centred cubic structure (space group Fm3m [225]) (JCPDS No. 87-0646),

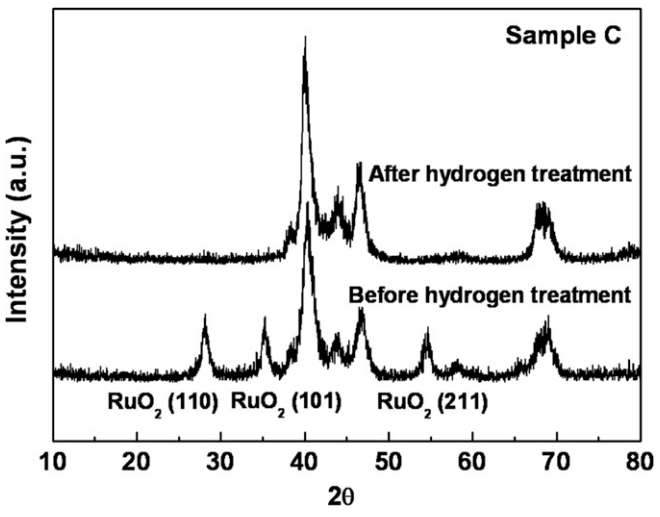

Fig. 5. Powder XRD plots obtained from sample C before and after the reduction process.

were observed at 39.7°, 46.2°, and 67.5°. In particular, diffraction peaks of sample D observed at 40.2°, 46.6°, and 68.0° are slightly shifted to the higher angle, which implies the formation of PtRu alloy, as previously reported in the literature [16]. That is, in the case of higher angle shift of Pt phases, PtRu alloy formation based on a substitution solid solution resulted from the different atomic size of the Pt and Ru atoms. Furthermore, to confirm the effect of the reduction process, XRD measurements were carried out before and after the reduction process for sample C as shown in Fig. 5. Although the diffraction peaks of sample C before the reduction process were observed as RuO_2 phases, there are no diffraction peaks relative to Ru oxide phases after the reduction process. Therefore, we demonstrated successful fabrication of PtRu/Ru core–shell NWs prepared from as-spun Ru/Pt NWs via co-electrospinning, and we confirmed their formation mechanism by means of SEM, TEM, EDS, and XRD.

4. Conclusion

PtRu/Ru core–shell NWs obtained from as-spun Ru/Pt core–shell NWs were successfully fabricated by means of a co-electrospinning method with a reduction process. Their structural properties were investigated together with the formation mechanism of the PtRu/Ru core–shell NWs, which is explained as the interdiffusion phenomenon by which Ru atoms move from the core region to the shell region and Pt atoms move from the shell region to the core region during calcination. This phenomenon may be attributed to the strong interaction between Ru atoms and the oxygen in air for Ru phases and to the easy formation of PtRu alloys between Pt atoms and Ru atoms for Pt phases.

Acknowledgment

This research was supported by Basic Science Research Program through the National Research Foundation of Korea (NRF) funded by the Ministry of Education, Science and Technology (2011-0005561).

References

[1] H. Weller, Angew. Chem. Int. Ed. 32 (1993) 41–53.
[2] Y. Xia, P. Yang, Y. Sun, Y. Wu, B. Mayers, B. Gates, Y. Yin, F. Kim, H. Yan, Adv. Mater. 15 (2003) 353–389.
[3] J.-B. Lee, S.-Y. Jeong, W.-J. Moon, T.-Y. Seong, H.-J. Ahn, J. Alloys Compd. 509 (2011) 4336–4340.
[4] S. Rmakrishna, K. Fujihara, W.E. Teo, T.C. Lim, Z. Ma, An Introduction to Electrospinning and Nanofibers, World Scientific Publishing Co. Ltd, Singapore, 2005.
[5] L. Dali, W. Guolei, D. Biao, B. Xue, W. Yu, S. Hongwei, X. Lin, Solid State Sci. 12 (2010) 1837–1842.
[6] W. Ponhan, S. Maensiri, Solid State Sci. 11 (2009) 479–484.
[7] Y. Zhang, Z.M. Huang, X. Xu, C.T. Lim, S. Ramakrishna, Chem. Mater. 16 (2004) 3406–3409.
[8] D. Li, Y. Xia, Nano. Lett. 4 (2004) 933–938.
[9] H. Chen, N. Wang, J. Di, Y. Zhao, Y. Song, L. Jiang, Langmuir 26 (2010) 11291–11296.
[10] Z. Sun, E. Zussman, A.L. Yarin, J.H. Wendorff, A. Greiner, Adv. Mater. 15 (2003) 1929–1932.
[11] Y.S. Kim, S.H. Nam, H.-S. Shim, H.-J. Ahn, M. Anand, W.B. Kim, Electrochem. Commun. 10 (2008) 1016–1019.
[12] P. Panagiotopoulou, D.I. Kondarides, X.E. Verykios, Appl. Catal. B Environ. 88 (2009) 470–478.
[13] G.-Y. Zhao, C.-L. Xu, H.-L. Li, Mater. Lett. 62 (2008) 1663–1665.
[14] R. Mukundan, E.L. Brosha, F.H. Garzon, Solid State Ionics 175 (2004) 497–501.
[15] W.F. Gale, T.C. Totemeier, Smithells Metals Reference Book, Elsevier Inc, Oxdord, UK, 2004.
[16] E.A. Baranova, Y.L. Page, D. Ilin, C. Bock, B. MacDougall, P.H.J. Mercier, J. Alloys Compd. 471 (2009) 387–394.